



Article

Exploring the Partonic Phase at Finite Chemical Potential in and out-of Equilibrium

O. Soloveva¹, P. Moreau^{1,2}, L. Oliva¹, V. Voronyuk^{3,4}, V. Kireyeu³, T. Song⁵ and E. Bratkovskaya^{1,5,*}

¹ Institut für Theoretische Physik, Goethe-Universität Frankfurt am Main, Frankfurt am Main, Germany; soloveva@fias.uni-frankfurt.de (O.S.); pierre.moreau@duke.edu (P.M.); oliva@fias.uni-frankfurt.de (L.O.)

² Department of Physics, Duke University, Durham, NC 27708, USA

³ Joint Institute for Nuclear Research, Joliot-Curie 6, 141980 Dubna, Moscow Region, Russia; vadim.voronyuk@jinr.ru (V.V.); vkireyeu@jinr.ru (V.K.)

⁴ Institute for Theoretical Physics, Metrolohichna str. 14-b, 03143 Kiev, Ukraine

⁵ GSI Helmholtzzentrum für Schwerionenforschung GmbH, Darmstadt, Germany; T.Song@gsi.de

* Correspondence: E.Bratkovskaya@gsi.de

Received: 15 January 2020; Accepted: 24 February 2020; Published: date



Abstract: We study the influence of the baryon chemical potential μ_B on the properties of the Quark–Gluon–Plasma (QGP) in and out-of equilibrium. The description of the QGP in equilibrium is based on the effective propagators and couplings from the Dynamical QuasiParticle Model (DQPM) that is matched to reproduce the equation-of-state of the partonic system above the deconfinement temperature T_c from lattice QCD. We study the transport coefficients such as the ratio of shear viscosity η and bulk viscosity ζ over entropy density s , i.e., η/s and ζ/s in the (T, μ) plane and compare to other model results available at $\mu_B = 0$. The out-of equilibrium study of the QGP is performed within the Parton–Hadron–String Dynamics (PHSD) transport approach extended in the partonic sector by explicitly calculating the total and differential partonic scattering cross sections based on the DQPM and the evaluated at actual temperature T and baryon chemical potential μ_B in each individual space-time cell where partonic scattering takes place. The traces of their μ_B dependences are investigated in different observables for symmetric Au+Au and asymmetric Cu+Au collisions such as rapidity and m_T -distributions and directed and elliptic flow coefficients v_1, v_2 in the energy range $7.7 \text{ GeV} \leq \sqrt{s_{NN}} \leq 200 \text{ GeV}$.

Keywords: hydrodynamic and kinetic approaches to dense matter

1. Introduction

The phase diagram of matter is one of the most fascinating subjects in physics, which also has important implications on chemistry and biology. Its phase boundaries and (possibly) critical points have been the focus of physics research for centuries. Apart from the traditional phase diagram in the plane of temperature T and pressure P , its transport properties like the shear and bulk viscosities, the electric conductivity, etc. are also of fundamental interest. These transport coefficients emerge from the stationary limit of correlators and provide additional information on the systems in thermal and chemical equilibrium apart from the equation of state. In this context, the phase diagram of strongly interacting matter has been the topic of most interest for decades and substantial experimental and theoretical efforts have been invested to shed light on this issue. It contains the information about the properties of our universe

from early beginning—directly after the Big Bang—when the matter was in the QGP phase at very large temperature T and about zero baryon chemical potential μ_B , to the later stages of the universe, where in the expansion phase stars and Galaxy have been formed. Here, the matter is at low temperature and large baryon chemical potential. Relativistic and ultra-relativistic heavy-ion collisions (HICs) nowadays offer the unique possibility to study some of these phases, in particular a QGP phase and its phase boundary to the hadronic one. Furthermore, the phase diagram of strongly interacting matter in the (T, μ_B) plane can also be explored in the astrophysical context at moderate temperatures and high μ_B [1], i.e., in the dynamics of supernovae or—more recently—in the dynamics of neutron star merges.

In order to reproduce the mini Big Bangs in laboratories, heavy-ion accelerators are built which allow for investigating the creation of the QGP under controlled conditions. Hadronic spectra and relative hadron abundances from these experiments reflect important aspects of the dynamics in the hot and dense zone formed in the early phase of the reaction and collective flows provide information on the transport properties of the medium generated on short time scales. Whereas heavy-ion reactions at Relativistic Heavy-Ion Collider (RHIC) and Large Hadron Collider (LHC) energies probe a partonic medium at small baryon chemical potential μ_B , the current interest is in collisions at lower bombarding energies where the net baryon density is higher and μ_B accordingly. Such conditions will be realized in future accelerators at the Facility for Antiproton and Ion Research (FAIR) in Darmstadt and the Nuclotron-based Ion Collider fAcility (NICA) in Dubna.

Current methods to explore QCD in Minkowski space for non-vanishing quark (or baryon) densities (or chemical potential) are effective approaches. Using effective models, one can study the dominant properties of QCD in equilibrium, i.e., thermodynamic quantities as well as transport coefficients. To this aim, the dynamical quasiparticle model (DQPM) has been introduced [2–6], which is based on partonic propagators with sizeable imaginary parts of the self-energies incorporated. Whereas the real part of the self-energies can be attributed to a dynamically generated mass (squared), the imaginary parts contain the information about the interaction rates in the system. Furthermore, the imaginary parts of the propagators define the spectral functions of the degrees of freedom which might show narrow (or broad) quasiparticle peaks. A further advantage of a propagator based approach is that one can formulate a consistent thermodynamics [7] as well as a causal theory for non-equilibrium configurations on the basis of Kadanoff–Baym equations [8].

In order to explore the properties of the QGP close to equilibrium, transport coefficients are calculated such as shear η and bulk ζ viscosities, electric conductivity σ_0 , etc. While basically all of the effective models have similar equations of state (EoS), which match well with available lattice QCD data at $\mu_B = 0$, the transport coefficients can vary significantly for different models (cf. [9]). Exploration of transport coefficients of the hot and dense QGP can provide useful information for simulations of heavy-ion collisions (HIC) based on hydrodynamical models for which they are used as input parameters. The experimental data for elliptic flow can be well reproduced by hydrodynamical simulations with a small value for the shear viscosity over entropy density [10,11].

Since relativistic heavy-ion collisions start with impinging nuclei in their groundstates, a proper non-equilibrium description of the entire dynamics through possibly different phases up to the final asymptotic hadronic states—eventually showing some degree of equilibration—is mandatory. To this aim, the Parton–Hadron–String Dynamics (PHSD) transport approach [5,12–15] has been formulated more than a decade ago (on the basis of the Hadron–String–Dynamics (HSD) approach [16]), and it was found to well describe observables from p+A and A+A collisions from SPS to LHC energies including electromagnetic probes such as photons and dileptons [5]. In order to explore the partonic systems at higher μ_B , the PHSD approach has been recently extended to incorporate partonic quasiparticles and their differential cross sections that depend not only on temperature T as in the previous PHSD studies, but also on chemical potential μ_B explicitly—cf. [17]. Within this extended approach, we have studied the

‘bulk’ observables in HIC for different energies—from AGS to RHIC, and systems—strongly asymmetric C+Au and symmetric Au+Au/Pb+Pb collisions. We have found only a small influence of μ_B dependences of parton properties (masses and widths) and their interaction cross sections in bulk observables [17].

In this work, we extend our study from Ref. [17] to the collective flow (v_1, v_2) coefficients and their sensitivity to the μ_B dependences of partonic cross sections. In addition, we explore the relations between the in and out-of equilibrium QGP by means of transport coefficients and collective flows. Additionally, we show explicitly the ‘bulk’ results for asymmetric heavy-ion collisions such as Cu+Au and discuss which hadronic species and observables are more sensitive to such effects.

2. The PHSD Approach

We start with reminding the basic ideas of the PHSD transport approach and the DQPM. The Parton–Hadron–String Dynamics transport approach [5,12–15] is a microscopic off-shell transport approach for the description of strongly interacting hadronic and partonic matter in and out-of equilibrium. It is based on the solution of Kadanoff–Baym equations in first-order gradient expansion [13] employing ‘resummed’ propagators from the dynamical quasiparticle model (DQPM) [2–4] for the partonic phase.

The Dynamical Quasiparticle Model (DQPM) has been introduced in Refs. [2–4] for the effective description of the properties of the QGP in terms of strongly interacting quarks and gluons with properties and interactions which are adjusted to reproduce IQCD results on the thermodynamics of the equilibrated QGP at finite temperature T and baryon (or quark) chemical potential μ_q . In the DQPM, the quasiparticles are characterized by single-particle Green’s functions (in propagator representation) with complex self-energies. The real part of the self-energies is related to the mean-field properties, whereas the imaginary part provides information about the lifetime and/or reaction rates of the particles.

In PHSD, the partons (quarks and gluons) are strongly interacting quasiparticles characterized by broad spectral functions ρ_j ($j = q, \bar{q}, g$), i.e., they are off-shell contrary to the conventional cascade or transport models dealing with on-shell particles, i.e., the δ -functions in the invariant mass squared. The quasiparticle spectral functions have a Lorentzian form [5] and depend on the parton mass and width parameters:

$$\rho_j(\omega, \mathbf{p}) = \frac{\gamma_j}{E_j} \left(\frac{1}{(\omega - E_j)^2 + \gamma_j^2} - \frac{1}{(\omega + E_j)^2 + \gamma_j^2} \right) \quad (1)$$

separately for quarks/antiquarks and gluons ($j = q, \bar{q}, g$). With the convention $E^2(\mathbf{p}^2) = \mathbf{p}^2 + M_j^2 - \gamma_j^2$, the parameters M_j^2 and γ_j are directly related to the real and imaginary parts of the retarded self-energy, e.g., $\Pi_j = M_j^2 - 2i\gamma_j\omega$.

The actual parameters in Equation (1), i.e., the gluon mass M_g and width γ_g —employed as input in the present PHSD calculations—as well as the quark mass M_q and width γ_q , are depicted in Figure 1 as a function of the temperature T and baryon chemical potential μ_B . These values for the masses and widths have been fixed by fitting the lattice QCD results from Ref. [35,36] in thermodynamic equilibrium. One can see that the masses of quarks and gluons decrease with increasing μ_B , and a similar trend holds for the widths of partons.

A scalar mean-field $U_s(\rho_s)$ for quarks and antiquarks can be defined by the derivative of the potential energy density with respect to the scalar density ρ_s ,

$$U_s(\rho_s) = \frac{dV_p(\rho_s)}{d\rho_s}, \quad (2)$$

which is evaluated numerically within the DQPM. Here, the potential energy density is defined by

$$V_p(T, \mu_q) = T_{g-}^{00}(T, \mu_q) + T_{q-}^{00}(T, \mu_q) + T_{\bar{q}-}^{00}(T, \mu_q), \quad (3)$$

where the different contributions T_{j-}^{00} correspond to the space-like part of the energy-momentum tensor component T_j^{00} of parton $j = g, q, \bar{q}$ (cf. Section 3 in Ref. [3]). The scalar mean-field $U_s(\rho_s)$ for quarks and antiquarks is repulsive as a function of the parton scalar density ρ_s and shows that the scalar mean-field potential is in the order of a few GeV for $\rho_s > 10 \text{ fm}^{-3}$. The mean-field potential (2) is employed in the PHSD transport calculations and determines the force on a partonic quasiparticle j , i.e., $\sim M_j/E_j \nabla U_s(x) = M_j/E_j dU_s/d\rho_s \nabla \rho_s(x)$, where the scalar density $\rho_s(x)$ is determined numerically on a space-time grid.

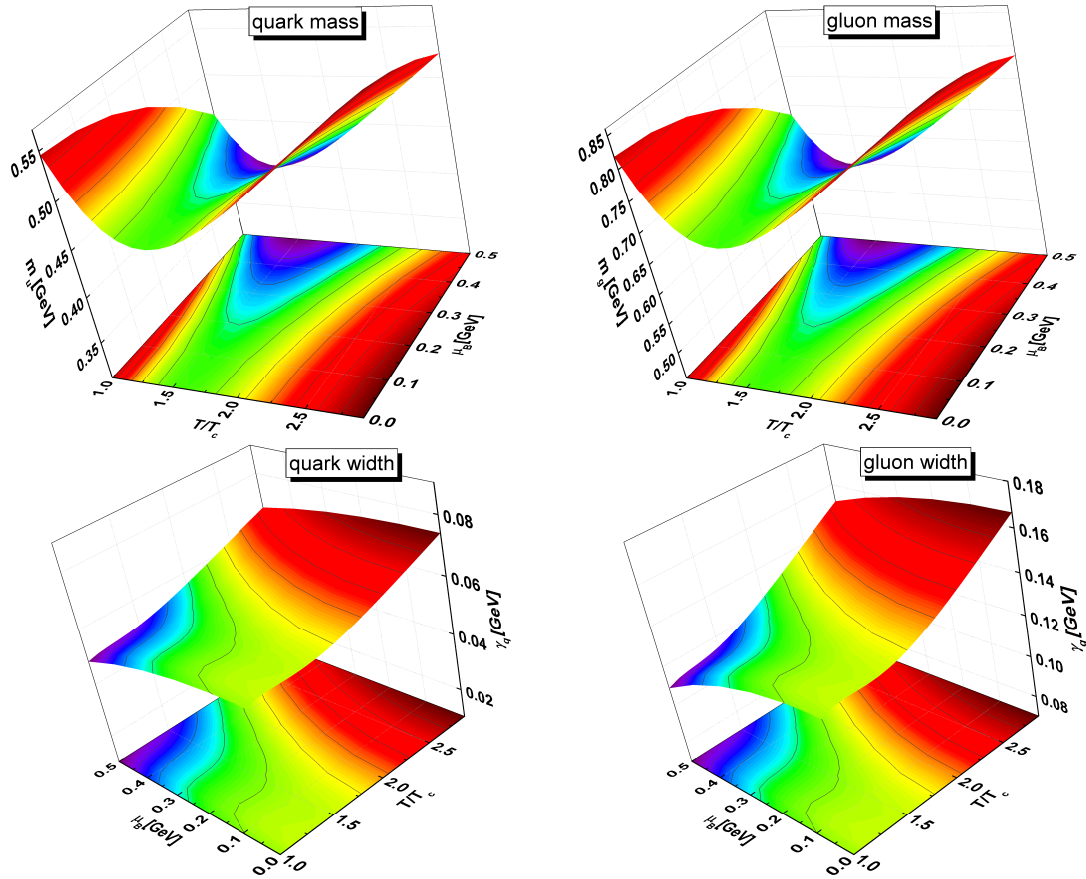


Figure 1. The effective quark (left) and gluon (right) masses M (upper row) and widths γ (lower row) as a function of the temperature T and baryon chemical potential μ_B .

Furthermore, a two-body interaction strength can be extracted from the DQPM as well from the quasiparticle width in line with Ref. [2]. On the partonic side, the following elastic and inelastic interactions are included in the latest version of PHSD (v. 5.0) $qq \leftrightarrow qq$, $\bar{q}\bar{q} \leftrightarrow \bar{q}\bar{q}$, $gg \leftrightarrow gg$, $gg \leftrightarrow g$, $q\bar{q} \leftrightarrow g$, $qg \leftrightarrow qg$, $g\bar{q} \leftrightarrow g\bar{q}$ exploiting ‘detailed-balance’ with cross sections calculated from the leading order Feynman diagrams employing the effective propagators and couplings $g^2(T/T_c)$ from the DQPM [17]. In Ref. [17], the differential and total off-shell cross sections have been evaluated as a function of the invariant energy of colliding off-shell partons \sqrt{s} for each T, μ_B . We remind that in the previous PHSD studies (using v. 4.0 and below) the cross sections depend only on T as evaluated in Ref. [18].

When implementing the differential cross sections and parton masses into the PHSD5.0 approach, one has to specify the ‘Lagrange parameters’ T and μ_B in each computational cell in space-time. This has been done by employing the lattice equation of state and a diagonalization of the energy-momentum tensor from PHSD as described in Ref. [17].

The transition from partonic to hadronic d.o.f. (and vice versa) is described by covariant transition rates for the fusion of quark–antiquark pairs or three quarks (antiquarks), respectively, obeying flavor current–conservation, color neutrality as well as energy–momentum conservation [14]. Since the dynamical quarks and antiquarks become very massive close to the phase transition, the formed resonant ‘prehadronic’ color-dipole states ($q\bar{q}$ or qqq) are of high invariant mass, too, and sequentially decay to the groundstate meson and baryon octets, thus increasing the total entropy.

On the hadronic side, PHSD includes explicitly the baryon octet and decuplet, the 0^- - and 1^- -meson nonets as well as selected higher resonances as in the Hadron–String–Dynamics (HSD) approach [16]. Note that PHSD and HSD (without explicit partonic degrees-of-freedom) merge at low energy density, in particular below the local critical energy density $\varepsilon_c \approx 0.5 \text{ GeV}/\text{fm}^3$.

3. Transport Coefficients

The transport properties of the QGP close to equilibrium can be characterized by various transport coefficients. The shear viscosity η and bulk viscosity ζ describe the fluid’s dissipative corrections at leading order. Both coefficients are generally expected to depend on the temperature T and baryon chemical potential μ_B . In the hydrodynamic equations, the viscosities appear as dimensionless ratios, η/s and ζ/s , where s is the fluid entropy density. Such specific viscosities are more meaningful than the unscaled η and ζ values because they describe the magnitude of stresses inside the medium relative to its natural scale.

In our recent studies [17,19,20], we have investigated the transport properties of the QGP in the (T, μ_B) plane based on the DQPM. One way to evaluate the viscosity coefficients of partonic matter is the Kubo formalism [21–24], which was used to calculate the viscosities for a previous version of the DQPM within the PHSD transport approach in a box with periodic boundary conditions in Ref. [25] as well as in the latest study with the DQPM model in Refs. [17,19]. Another way to calculate transport coefficients (explored also in [17,19]) is to use the relaxation–time approximation (RTA) [26–29].

The shear viscosity based on the RTA (cf. [30]) reads as:

$$\eta^{\text{RTA}}(T, \mu_q) = \frac{1}{15T} \sum_{i=q,\bar{q},g} \int \frac{d^3p}{(2\pi)^3} \frac{\mathbf{p}^4}{E_i^2} \tau_i(\mathbf{p}, T, \mu) d_i (1 \pm f_i) f_i, \quad (4)$$

where $d_q = 2N_c = 6$ and $d_g = 2(N_c^2 - 1) = 16$ are degeneracy factors for spin and color in case of quarks and gluons, τ_i are relaxation times. Equation (4) includes the Bose enhancement and Pauli-blocking factors, respectively. The pole energy is $E_i^2 = p^2 + M_i^2$, where M_i is the pole mass given in the DQPM. The notation $\sum_{i=q,\bar{q},g}$ includes the contribution from all possible partons which in our case are the gluons and the (anti-)quarks of three different flavors (u, d, s).

We consider two cases for the relaxation time for quarks and gluons: (1) $\tau_i(\mathbf{p}, T, \mu) = 1/\Gamma_i(\mathbf{p}, T, \mu)$ and (2) $\tau_i(T, \mu) = 1/2\gamma_i(T, \mu)$, where $\Gamma_i(\mathbf{p}, T, \mu)$ is the parton interaction rate, calculated microscopically from the collision integral using the differential cross sections for parton scattering, while $\gamma_i(T, \mu)$ is the width parameter in the parton propagator (1).

In the left part (a) of Figure 2, we show the ratio of the shear viscosity to entropy density as a function of the scaled temperature T/T_c for $\mu_B = 0$ calculated using the Kubo formalism (green solid line) and RTA approach with the interaction rate Γ^{on} (red solid line) and the DQPM width 2γ (dashed green line). The RTA approximation (4) of the shear viscosity with the DQPM width 2γ and with the interaction rate

Γ^{on} are quite close to each other at $\mu_B = 0$ and also very close to the one from the Kubo formalism [17] indicating that the quasiparticle limit ($\gamma \ll M$) holds in the DQPM.

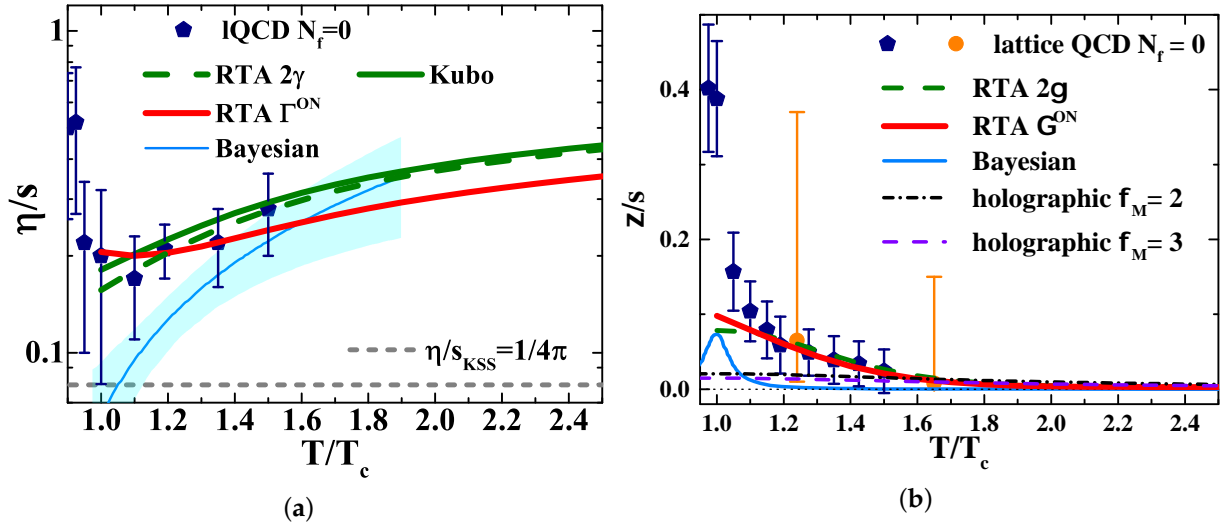


Figure 2. Left (a): the ratio of shear viscosity to entropy density as a function of the scaled temperature T/T_c for $\mu_B = 0$ calculated using the Kubo formalism (green solid line) and the RTA approach with the interaction rate Γ^{on} (red solid line) and the DQPM width 2γ (dashed green line). The dashed gray line demonstrates the Kovtun–Son–Starinets bound [31] ($\eta/s_{\text{KSS}} = 1/(4\pi)$), and the symbols show IQCD data for pure SU(3) gauge theory taken from Ref. [32] (pentagons). The solid blue line shows the results from a Bayesian analysis of experimental heavy-ion data from Ref. [34]. Right (b): the ratio of the bulk viscosity to entropy density ζ/s as a function of the scaled temperature T/T_c for $\mu_B = 0$ calculated using the RTA approach with the on-shell interaction rate Γ^{on} (red solid line) and the DQPM width 2γ (dashed green line). The symbols correspond to the IQCD data for pure SU(3) gauge theory taken from Refs. [33] (pentagons) and [37] (circles). The solid blue line shows the results from a Bayesian analysis of experimental heavy-ion data from Ref. [34]. The dot-dashed and dashed lines correspond to the results from the non-conformal holographic model for $\phi_M = 2$ and 3, correspondingly, from Ref. [39].

The ratio η/s increases with an increase of the scaled temperature. The actual values for the ratio η/s are in a good agreement with the gluodynamic lattice QCD calculations at $\mu_B = 0$ from Ref. [32]. Moreover, our DQPM results are in qualitative agreement with the results from a Bayesian analysis of experimental heavy-ion data from Ref. [34]. We mention that the DQPM result differs from the recent calculations for the shear viscosity at $\mu_B = 0$ in the quasiparticle model in Ref. [38] where the width of quasiparticles is not considered which leads to a high value for the η/s ratio. This shows the sensitivity of this ratio to the modelling of partonic interactions and the properties of partons in the hot QGP medium. We remind also that in Refs. [17,19,20] we find that the ratio η/s shows a very weak dependence on μ_B and has a similar behavior as a function of temperature for all $\mu_B \leq 400$ MeV.

The expression for the bulk viscosity of the partonic phase derived within the RTA reads (following Ref. [28])

$$\zeta^{\text{RTA}}(T, \mu) = \frac{1}{9T} \sum_{i=q,\bar{q},g} \int \frac{d^3p}{(2\pi)^3} \tau_i(\mathbf{p}, T, \mu) \frac{d_i(1 \pm f_i)f_i}{E_i^2} \left(\mathbf{p}^2 - 3c_s^2 \left(E_i^2 - T^2 \frac{dm_i^2}{dT^2} \right) \right)^2, \quad (5)$$

where c_s^2 is the speed of sound squared, and $\frac{dm_i^2}{dT^2}$ is the DQPM parton mass derivative which becomes large close to the critical temperature T_c .

On the right side (b) of Figure 2, we show the ratio of the bulk viscosity to entropy density ζ/s as a function of the scaled temperature T/T_c for $\mu_B = 0$ calculated using the RTA approach with the interaction rate Γ^{on} (red solid line) and the DQPM width 2γ (dashed green line). The symbols correspond to the lQCD data for pure SU(3) gauge theory taken from Refs. [33] (pentagons) and [37] (circles). The solid blue line shows the results from a Bayesian analysis of experimental heavy-ion data from Ref. [34]. The dot-dashed and dashed lines correspond to the results from the non-conformal holographic model [39] for $\phi_M = 2$ and 3, correspondingly, where ϕ_M is the model parameter which characterizes the non-conformal features of the model. We find that the DQPM result for ζ/s is in very good agreement with the lattice QCD results and shows a rise closer to T_c contrary to the holographic results, which show practically a constant behavior independent of model parameters. This rise is attributed to the increase of the partonic mass closer to T_c as shown in Figure 1, thus the mass derivative term in Equation (5) also grows. The Bayesian result also shows a peak near T_c ; however, the ratio drops to zero while lQCD data indicate the positive ζ/s as found also in the DQPM. The μ_B dependence of ζ/s has been investigated within the DQPM in Refs. [17,19,20], where it has been shown that it is rather weak for $\mu_B \leq 400$ MeV, similar to η/s . As follows from hydrodynamical calculations, the results for the flow harmonic v_n is sensitive to the transport coefficients [10,11,34]. Thus, there are hopes to observe a μ_B sensitivity of v_1, v_2 .

4. Heavy-Ion Collisions

In our recent study [17], we have investigated the sensitivity of ‘bulk’ observables such as rapidity and transverse momentum distributions of different hadrons produced in heavy-ion collisions from AGS to top RHIC energies on the details of the QGP interactions and the properties of partonic degrees-of-freedom. For that, we have considered the following three cases:

(1) ‘PHSD4.0’: the masses and widths of quarks and gluons depend only on T . The cross sections for partonic interactions depend only on T as evaluated in the ‘box’ calculations in Ref. [18] in order to merge the QGP interaction rates from all possible partonic channels to the total temperature dependent widths of the DQPM propagator. This has been used in the PHSD code (v. 4.0 or below) for extended studies of many hadronic observables in p+A and A+A collisions at different energies [5,12–15,40].

(2) ‘PHSD5.0 - $\mu_B = 0$ ’: the masses and widths of quarks and gluons depend only on T ; however, the differential and total partonic cross sections are obtained by calculations of the leading order Feynman diagrams employing the effective propagators and couplings $g^2(T/T_c)$ from the DQPM at $\mu_B = 0$ [17]. Thus, the cross sections depend explicitly on the invariant energy of the colliding partons \sqrt{s} and on T . This is realized in the PHSD5.0 by setting $\mu_B = 0$, cf. [17].

(3) ‘PHSD5.0 - μ_B ’: the masses and widths of quarks and gluons depend on T and μ_B explicitly; the differential and total partonic cross sections are obtained by calculations of the leading order Feynman diagrams from the DQPM and explicitly depend on invariant energy \sqrt{s} , temperature T and baryon chemical potential μ_B . This is realized in the full version of PHSD5.0, cf. [17].

The comparison of the ‘bulk’ observables for A+A collisions within the three cases of PHSD in Ref. [17] has illuminated that they show a very low sensitivity to the μ_B dependences of parton properties (masses and widths) and their interaction cross sections such that the results from PHSD5.0 with and without μ_B were very close to each other. Only in the case of kaons, antiprotons \bar{p} and antihyperons $\bar{\Lambda} + \bar{\Sigma}^0$, a small difference between PHSD4.0 and PHSD5.0 could be seen at top SPS and top RHIC energies. A similar trend has been found for very asymmetric collisions of C+Au: a small sensitivity to the partonic scatterings was found in the kaon and antibaryon rapidity distributions too. This could be understood as following: at high energies such as top RHIC where the QGP volume is very large in central collisions, the μ_B is very low, while, when decreasing the bombarding energy—in order to increase μ_B , the fraction of the QGP is decreasing such that the final observables are dominated by the hadronic phase, i.e., the probability for the

hadrons created at the QGP hadronization to re-scatter, decay, or be absorbed in hadronic matter increases strongly; accordingly, the sensitivity to the properties of the QGP is washed out.

4.1. Asymmetric Systems

In Ref. [17], we have investigated the sensitivity to μ_B of the ‘bulk’ observables in asymmetric heavy-ion collisions for C+Au. The spectra for C+Au indicated that they show a slightly larger sensitivity to μ_B for antiprotons and strange hadrons, kaons and antihyperons than for pions and protons. Here, we present the results for the asymmetric Cu+Au collisions.

In Figures 3 and 4, we show the rapidity distributions (left plot) and p_T -spectra at midrapidity ($|y| < 0.5$) (right plot) for $\pi^\pm, K^\pm, p, \bar{p}, \Lambda + \Sigma^0, \bar{\Lambda} + \bar{\Sigma}^0$ for 10% central Cu+Au collisions at 30 AGeV and $\sqrt{s_{NN}} = 200$ GeV for three cases: (1) PHSD4.0 (green dot-dashed lines), (2) PHSD5.0 with partonic cross sections and parton masses/widths calculated for $\mu_B = 0$ (blue dashed lines) and (3) with cross sections and parton masses/widths evaluated at the actual chemical potential μ_B in each individual space-time cell (red lines). Similar to C+Au collisions, we find for Cu+Au collisions a small difference in the rapidity distributions of antiprotons and in the strangeness sector - in kaon and especially in $\bar{\Lambda} + \bar{\Sigma}^0$ y -distributions. Similar statements hold for the p_T spectra which show a slightly different slope at low and high momenta of anti-strange baryons. This suggests that the strange degree-of-freedom might be experimentally explored in asymmetric systems to obtain additional information on the partonic interactions.

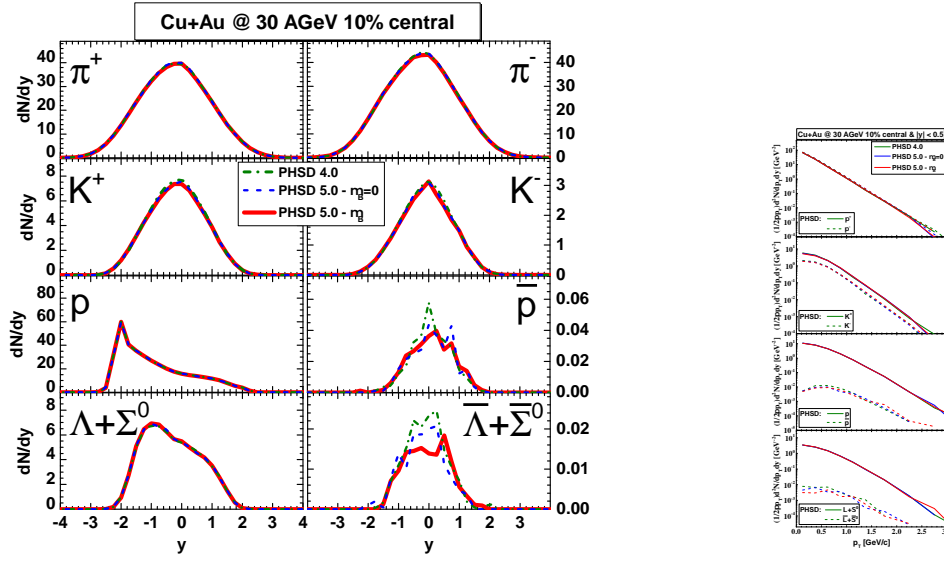


Figure 3. The rapidity distributions (left plot) and p_T -spectra at midrapidity ($|y| < 0.5$) (right plot) for $\pi^\pm, K^\pm, p, \bar{p}, \Lambda + \Sigma^0, \bar{\Lambda} + \bar{\Sigma}^0$ for 10% central Cu+Au collisions at 30 A GeV for PHSD4.0 (green dot-dashed lines), PHSD5.0 with partonic cross sections and parton masses calculated for $\mu_B = 0$ (blue dashed lines) and with cross sections and parton masses evaluated at the actual chemical potential μ_B in each individual space-time cell (red lines).

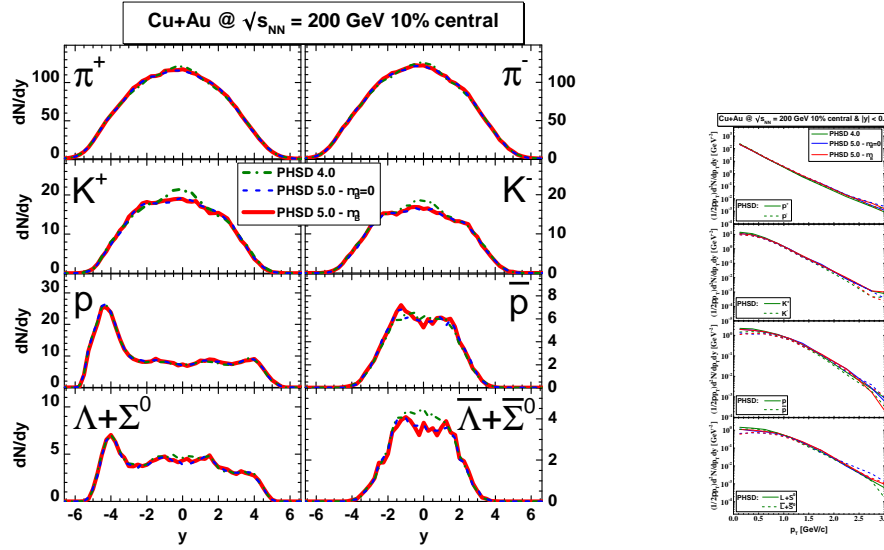


Figure 4. The rapidity distributions (left plot) and p_T -spectra at midrapidity ($|y| < 0.5$) (right plot) for $\pi^\pm, K^\pm, p, \bar{p}, \Lambda + \Sigma^0, \bar{\Lambda} + \bar{\Sigma}^0$ for 10% central Cu+Au collisions at $\sqrt{s_{NN}} = 200$ GeV for PHSD4.0 (green dot-dashed lines), PHSD5.0 with partonic cross sections and parton masses calculated for $\mu_B = 0$ (blue dashed lines) and with cross sections and parton masses evaluated at the actual chemical potential μ_B in each individual space-time cell (red lines).

4.2. Directed Flow

Now, we test the traces of μ_B dependences of the QGP interaction cross sections in collective observables such as directed flow v_1 considering again three cases of the PHSD as discussed above.

Figure 5 depicts the directed flow v_1 of identified hadrons ($K^\pm, p, \bar{p}, \Lambda + \Sigma^0, \bar{\Lambda} + \bar{\Sigma}^0$) versus rapidity for $\sqrt{s_{NN}} = 27$ GeV. One can see a good agreement between PHSD results and experimental data from STAR collaboration [41]. However, the different versions of PHSD for the v_1 coefficient show a quite similar behavior; only antihyperons show a slightly different flow. This supports again the finding that strangeness, and in particular anti-strange hyperons, are the most sensitive probes for the QGP properties.

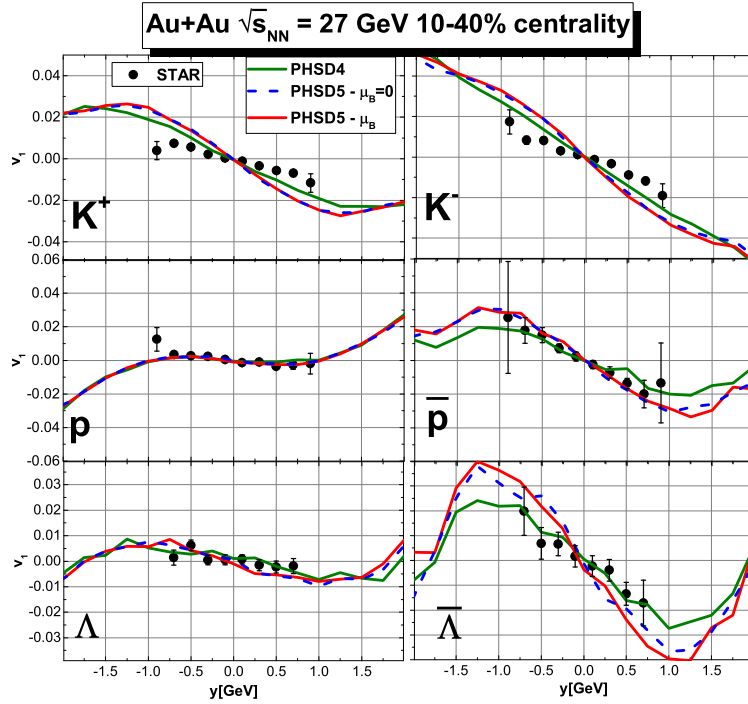


Figure 5. Directed flow of identified hadrons as a function of rapidity at $\sqrt{s_{NN}} = 27$ GeV for PHSD4.0 (green lines), PHSD5.0 with partonic cross sections and parton masses calculated for $\mu_B = 0$ (blue dashed lines) and with cross sections and parton masses evaluated at the actual chemical potential μ_B in each individual space-time cell (red lines) in comparison to the experimental data of the STAR Collaboration [41].

4.3. Elliptic Flow

As follows from the hydrodynamic simulations [10,11] and from the Bayesian analysis [34], an elliptic flow v_2 is sensitive to the transport properties of the QGP characterized by transport coefficients such as shear η and bulk ζ viscosities. In this section, we present the results for the elliptic flow of charged hadrons from HIC within the PHSD5.0 with and without μ_B dependences and compare the results with PHSD4.0, again.

The left plots ‘(a)’ in Figures 6 and 7 display the actual results for charged hadron elliptic flow as a function of pseudo-rapidity η (Figure 6) and of transverse momentum p_T (Figure 7) for minimum bias Au+Au collisions at $\sqrt{s_{NN}} = 200$ GeV for PHSD4.0 (green lines), PHSD5.0 with partonic cross sections and parton masses calculated for $\mu_B = 0$ (blue dashed lines), and with cross sections and parton masses evaluated at the actual chemical potential μ_B in each individual space-time cell (red lines) in comparison to the experimental data from the STAR collaboration [42] (solid stars) and PHOBOS [44] (solid dots). One can see the difference for $v_2(p_T)$ in case of charged hadrons for high $p_T > 0.5$ GeV between PHSD4.0 and PHSD5.0.

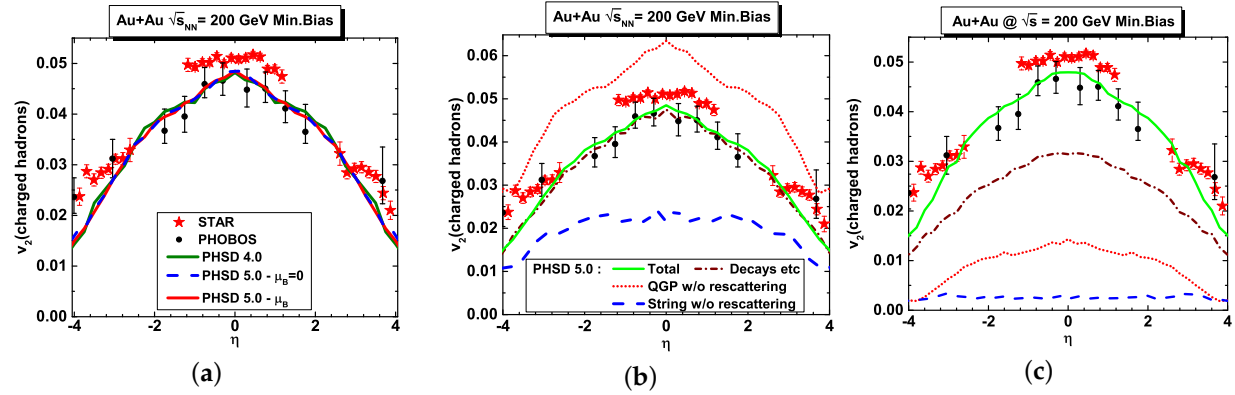


Figure 6. Left (a): elliptic flow of charged hadrons as function of pseudo-rapidity η for minimum bias Au+Au collisions at $\sqrt{s_{NN}}=200$ GeV for PHSD4.0 (green lines), PHSD5.0 with partonic cross sections and parton masses calculated for $\mu_B = 0$ (blue dashed lines), and with the actual μ_B (red lines) in comparison to the experimental data from STAR [42] (solid starts) and PHOBOS [44] (solid dots). Middle (b): individual contributions to v_2 without their relative weights to the total v_2 , which are indicated by a green solid line for PHSD5.0 with μ_B : the red dotted line corresponds to the final hadrons coming from the QGP without rescattering in the hadronic phase, the blue dashed line indicates the v_2 of hadrons coming from strings while the brown dot-dashed line shows the v_2 of hadrons coming from mesonic and baryonic resonance decays. Right (c): individual contributions to v_2 including their relative weights to the total v_2 .

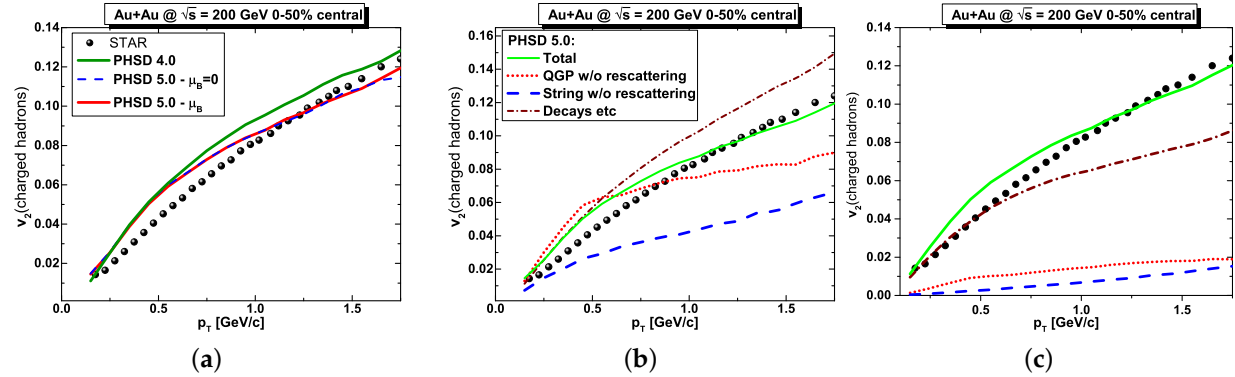


Figure 7. Elliptic flow of charged hadrons as a function of p_T for 0–50% central Au+Au collisions at $\sqrt{s_{NN}} = 200$ GeV. The line description is similar to Figure 6.

The channel composition of v_2 for PHSD5.0—with cross sections and parton masses evaluated at the actual chemical potential μ_B in each individual space-time cell—is shown in the middle plots ‘(b)’ of Figures 6 and 7. We sorted the particles according to their production channels into three parts: the red dotted line corresponds to the final hadrons coming from the QGP without rescattering in the hadronic phase, the blue dashed line indicates the v_2 of hadrons coming from strings (without further rescattering) while the brown dot-dashed line shows the v_2 of hadrons coming from mesonic and baryonic resonance decays. One can see a large difference between the averaged elliptic flow for the different channels: the v_2 of hadrons from string decay is the lowest since string production occurs dominantly at the initial phase of the heavy-ion collision; the v_2 of hadrons from the QGP is the largest versus η as follows from the middle Part ‘(b)’ of Figure 6. However, this is mainly due to the low p_T hadrons which give a larger contribution to $v_2(\eta)$ —cf. the middle part ‘(b)’ of Figure 7. Here, the high p_T hadrons from the QGP show a lower v_2 than those coming from strings or resonance decays.

The right parts ‘(c)’ of Figures 6 and 7 present the individual contributions to v_2 including their relative weights to the total v_2 . It shows that the properly weighted channel decomposition of v_2 looks rather different—the contribution of the hadrons from the QGP is now small since most of them rescatter in the hadronic phase, i.e., the relative fraction of hadrons directly coming from QGP hadronization is very small. The total v_2 is dominated by the hadrons coming from the decay of resonances. The fraction of hadrons from string decays is very small due to the fact that strings are formed mainly in the beginning of collisions, and a very small fraction of hadrons can survive directly. Thus, the information in v_2 about the QGP properties is washed out to a large extent by final hadronic interactions.

In Figure 8, we present the elliptic flow of identified hadrons ($K^\pm, p, \bar{p}, \Lambda + \Sigma^0, \bar{\Lambda} + \bar{\Sigma}^0$) as a function of p_T at $\sqrt{s_{NN}} = 27$ GeV for PHSD4.0 (green lines), PHSD5.0 with partonic cross sections and parton masses calculated for $\mu_B = 0$ (blue dashed lines) and with cross sections and parton masses evaluated at the actual chemical potential μ_B in each individual space-time cell (red lines) in comparison to the experimental data of the STAR Collaboration [43]. Similar to the directed flow shown in Figure 5, the elliptic flow from all three cases for PHSD shows a rather similar behavior, the differences are very small (within the statistics achieved here). Only antiprotons and antihyperons show a small decrease of v_2 at larger p_T for PHSD5.0 compared to PHSD4.0, which can be attributed to the explicit \sqrt{s} -dependence and different angular distribution of partonic cross sections in the PHSD5.0. We note that the underestimation of v_2 for protons and Λ ’s we attribute to the details of the hadronic vector potential involved in this calculations which seems to underestimate repulsion.

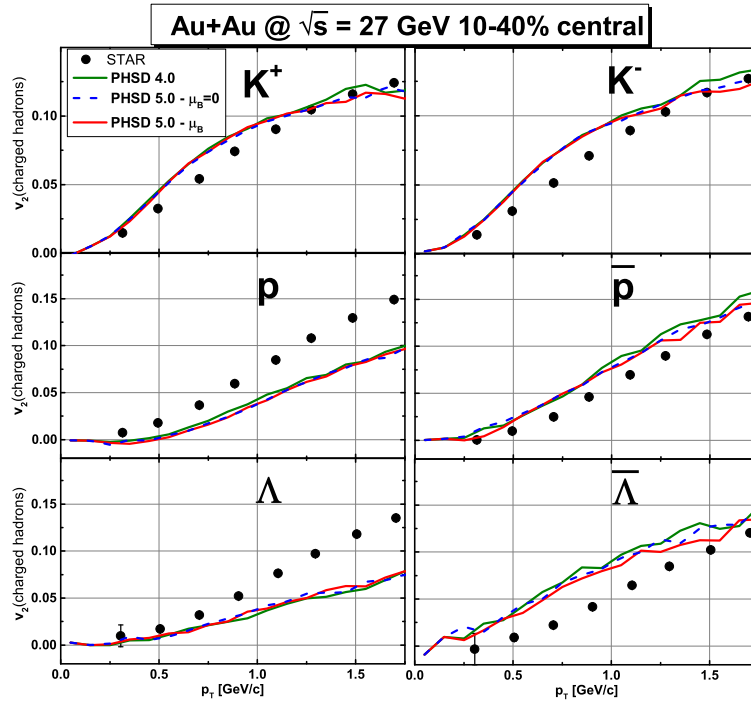


Figure 8. Elliptic flow of identified hadrons ($K^\pm, p, \bar{p}, \Lambda + \Sigma^0, \bar{\Lambda} + \bar{\Sigma}^0$) as a function of p_T at $\sqrt{s_{NN}} = 27$ GeV for PHSD4.0 (green lines), PHSD5.0 with partonic cross sections and parton masses calculated for $\mu_B = 0$ (blue dashed lines) and with cross sections and parton masses evaluated at the actual chemical potential μ_B in each individual space-time cell (red lines) in comparison to the experimental data of the STAR Collaboration [43].

5. Conclusions

In this work, we have studied the influence of the baryon chemical potential μ_B on the properties of the QGP in equilibrium as well as the QGP created in heavy-ion collisions also far from equilibrium.

For the description of the QGP, we employed the extended effective Dynamical QuasiParticle Model (DQPM) that is matched to reproduce the IQCD crossover equation-of-state versus temperature T and at finite baryon chemical potential μ_B . We compared the DQPM results for transport coefficients such as shear viscosity η and bulk viscosity ζ with available IQCD data and the non-conformal holographic model at $\mu_B = 0$ and with results from a Bayesian analysis of experimental heavy-ion data. We find that the ratios η/s and ζ/s from the DQPM agree very well with the IQCD results from Ref. [33] and show a similar behavior as the ratio obtained from a Bayesian fit [34]. As found in [17,19], the transport coefficients show a mild dependence on μ_B .

Following [17], we based our study of the non-equilibrium QGP—as created in heavy-ion collisions—on the extended Parton–Hadron–String Dynamics (PHSD) transport approach in which i) the masses and widths of quarks and gluons depend on T and μ_B explicitly; ii) the partonic interaction cross sections are obtained by calculations of the leading order Feynman diagrams from the DQPM and explicitly depend on the invariant energy \sqrt{s} , temperature T and baryon chemical potential μ_B . This extension is realized in the full version of PHSD5.0 [17].

In order to investigate the traces of the μ_B dependence of the QGP in observables, the results of PHSD5.0 with μ_B dependences have been compared to the results of PHSD5.0 for $\mu_B = 0$ as well as with PHSD4.0 where the masses/width of quarks and gluons as well as their interaction cross sections depend only on T following Ref. [18]. We have presented the PHSD results for different observables: (i) rapidity and p_T distributions of identified hadrons for asymmetric Cu+Au collisions at energies of 30 AGeV (future NICA energy) as well as for the top RHIC energy of $\sqrt{s_{NN}} = 200$ GeV; (ii) directed flow v_1 of identified hadrons for $Au + Au$ at invariant energy $\sqrt{s_{NN}} = 27$ GeV; (iii) elliptic flow v_2 of identified hadrons for $Au + Au$ at invariant energies $\sqrt{s_{NN}} = 27$ and 200 GeV. We find only small differences between PHSD4.0 and PHSD5.0 results on the hadronic observables considered here at high as well as at intermediate energies. This is related to the fact that at high energies, where the matter is dominated by the QGP, one probes a very small baryon chemical potential in central collisions at midrapidity, while, with decreasing energy, where μ_B becomes larger, the fraction of the QGP drops rapidly, such that in total the final observables are dominated by the hadrons which participated in hadronic rescattering and thus the information about their QGP origin is washed out. We have shown that the μ_B dependence of QGP interactions is more pronounced in observables for strange hadrons, kaons and especially anti-strange hyperons, as well as for antiprotons. This gives an experimental hint for the searching of μ_B traces of the QGP for experiments at the future NICA accelerator, even if it will be a very challenging experimental task.

Acknowledgments: The authors acknowledge inspiring discussions with J. Aichelin, W. Cassing, V. Kolesnikov, I. Selyuzhenkov and A. Taranenko. We thank M. Attems for providing us the results from Ref. [38] in data form. Furthermore, we acknowledge support by the Deutsche Forschungsgemeinschaft (DFG, German Research Foundation) through the grant CRC-TR 211 ‘Strong-interaction matter under extreme conditions’ - Project number 315477589 - TRR 211. O.S. acknowledges support from HGS-HiRe for FAIR; L.O. and E.B. thank the COST Action THOR, CA15213. L.O. has been financially supported in part by the Alexander von Humboldt Foundation. The computational resources have been provided by the LOEWE-Center for Scientific Computing.

Conflicts of Interest: The authors declare no conflict of interest.

References

1. Klahn, T.; Blaschke, D.; Typel, S.; Van Dalen, E.N.E.; Faessler, A.; Fuchs, C.; Gaitanos, T.; Grigorian, H.; Ho, A.; Kolomeitsev, E.E.; et al. Constraints on the high-density nuclear equation of state from the phenomenology of compact stars and heavy-ion collisions. *Phys. Rev. C* **2006**, *74*, 035802.
2. Peshier, A.; Cassing, W. The hot non-perturbative gluon plasma is an almost ideal colored liquid. *Phys. Rev. Lett.* **2005**, *94*, 172301.
3. Cassing, W. Dynamical quasiparticles properties and effective interactions in the sQGP. *Nucl. Phys. A* **2007**, *795*, 70–97.
4. Cassing, W. QCD thermodynamics and confinement from a dynamical quasiparticle point of view. *Nucl. Phys. A* **2007**, *791*, 365–381.
5. Linnyk, O.; Bratkovskaya, E.L.; Cassing, W. Effective QCD and transport description of dilepton and photon production in heavy-ion collisions and elementary processes. *Prog. Part. Nucl. Phys.* **2016**, *87*, 50–115.
6. Berrehrah, H.; Bratkovskaya, E.; Steinert, T.; Cassing, W. A dynamical quasiparticle approach for the QGP bulk and transport properties. *Int. J. Mod. Phys. E* **2016**, *25*, 1642003.
7. Vanderheyden, B.; Baym, G. Selfconsistent approximations in relativistic plasmas: Quasiparticle analysis of the thermodynamic properties. *J. Stat. Phys.* **1998**, *93*, 843–861.
8. Kadanoff, L.P.; Baym, G. *Quantum Statistical Mechanics*; W. A. Benjamin, Inc.: New York, NY, USA, 1962.
9. Marty, R.; Bratkovskaya, E.; Cassing, W.; Aichelin, J.; Berrehrah, H. Transport coefficients from the Nambu-Jona-Lasinio model for $SU(3)_f$. *Phys. Rev. C* **2013**, *88*, 045204.
10. Romatschke, P.; Romatschke, U. Viscosity Information from Relativistic Nuclear Collisions: How Perfect is the Fluid Observed at RHIC? *Phys. Rev. Lett.* **2007**, *99*, 172301.
11. Song, H.; Heinz, U.W. Multiplicity scaling in ideal and viscous hydrodynamics. *Phys. Rev. C* **2008**, *78*, 024902.
12. Cassing, W.; Bratkovskaya, E.L. Parton transport and hadronization from the dynamical quasiparticle point of view. *Phys. Rev. C* **2008**, *78*, 034919.
13. Cassing, W. From Kadanoff–Baym dynamics to off-shell parton transport. *Eur. Phys. J. Spec. Top.* **2009**, *168*, 3–87.
14. Cassing, W.; Bratkovskaya, E.L. Parton–Hadron–String Dynamics: An off-shell transport approach for relativistic energies. *Nucl. Phys. A* **2009**, *831*, 215.
15. Bratkovskaya, E.L.; Cassing, W.; Konchakovski, V.P.; Linnyk, O. Parton–Hadron–String Dynamics at Relativistic Collider Energies. *Nucl. Phys. A* **2011**, *856*, 162–182.
16. Cassing, W.; Bratkovskaya, E.L. Hadronic and electromagnetic probes of hot and dense nuclear matter. *Phys. Rep.* **1999**, *308*, 65–233.
17. Moreau, P.; Soloveva, O.; Oliva, L.; Song, T.; Cassing, W.; Bratkovskaya, E. Exploring the partonic phase at finite chemical potential within an extended off-shell transport approach. *Phys. Rev. C* **2019**, *100*, 014911.
18. Ozvenchuk, V.; Linnyk, O.; Gorenstein, M.I.; Bratkovskaya, E.L.; Cassing, W. Dynamical equilibration of strongly interacting “infinite” parton matter within the parton–hadron–string dynamics transport approach. *Phys. Rev. C* **2013**, *87*, 024901.
19. Soloveva, O.; Moreau, P.; Bratkovskaya, E. Transport coefficients for the hot quark-gluon plasma at finite chemical potential μ_B . *arXiv* **2019**, arXiv:1911.08547.
20. Soloveva, O.; Moreau, P.; Oliva, L.; Song, T.; Cassing, W.; Bratkovskaya, W. Transport coefficients of hot and dense matter. *arXiv* **2019**, arXiv:1911.03131.
21. Kubo, R. Statistical mechanical theory of irreversible processes. 1. General theory and simple applications in magnetic and conduction problems. *J. Phys. Soc. Jpn.* **1957**, *12*, 570–586.
22. Aarts G.; Martinez Resco, J.M. Transport coefficients, spectral functions and the lattice. *J. High Energy Phys.* **2002**, *204*, 053.
23. Fernandez-Fraile, D.; Gomez Nicola, A. The Electrical conductivity of a pion gas. *Phys. Rev. D* **2006**, *73*, 045025.
24. Lang, R.; Kaiser, N.; Weise, W. Shear viscosities from Kubo formalism in a large- N_c Nambu-Jona-Lasinio model. *Eur. Phys. J. A* **2015**, *51*, 127.

25. Ozvenchuk, V.; Linnyk, O.; Gorenstein, M.I.; Bratkovskaya, E.L.; Cassing, W. Shear and bulk viscosities of strongly interacting “infinite” parton-hadron matter within the Parton–Hadron–String dynamics transport approach. *Phys. Rev. C* **2013**, *87*, 064903.
26. Hosoya, A.; Kajantie, K. Transport Coefficients of QCD Matter. *Nucl. Phys. B* **1985**, *250*, 666–688.
27. Chakraborty, P.; Kapusta, J.I. Quasi-Particle Theory of Shear and Bulk Viscosities of Hadronic Matter. *Phys. Rev. C* **2011**, *83*, 014906.
28. Albright, M.; Kapusta, J.I. Quasiparticle Theory of Transport Coefficients for Hadronic Matter at Finite Temperature and Baryon Density. *Phys. Rev. C* **2016**, *93*, 014903.
29. Gavin, S. Transport Coefficients In Ultrarelativistic Heavy Ion Collisions. *Nucl. Phys. A* **1985**, *435*, 826–843.
30. Sasaki, C.; Redlich, K. Bulk viscosity in quasi particle models. *Phys. Rev. C* **2009**, *79*, 055207.
31. Kovtun, P.K.; Son, D.T.; Starinets, A.O. Viscosity in strongly interacting quantum field theories from black hole physics. *Phys. Rev. Lett.* **2005**, *94*, 111601.
32. Astrakhantsev, N.; Braguta, V.; Kotov, A. Temperature dependence of shear viscosity of SU(3)–gluodynamics within lattice simulation. *Phys. J. High Energy Phys.* **2017**, *4*, 101.
33. Astrakhantsev, N.Y.; Braguta, V.V.; Kotov, A.Y. Temperature dependence of the bulk viscosity within lattice simulation of SU(3) gluodynamics. *Phys. Rev. D* **2018**, *98*, 054515.
34. Bernhard, J.E.; Moreland, J.S.; Bass, S.A.; Liu, J.; Heinz, U. Applying Bayesian parameter estimation to relativistic heavy-ion collisions: simultaneous characterization of the initial state and quark-gluon plasma medium. *Phys. Rev. C* **2016**, *94*, 024907.
35. Borsanyi, S.; Endrodi, G.; Fodor, Z.; Katz, S.D.; Krieg, S.; Ratti, C.; Szabo, K.K. QCD equation of state at nonzero chemical potential: Continuum results with physical quark masses at order μ^2 . *J. High Energy Phys.* **2012**, *1208*, 053.
36. Borsanyi, S.; Fodor, Z.; Hoelbling, C.; Katz, S.D.; Krieg, S.; Szabo, K.K. Full result for the QCD equation of state with 2+1 flavors. *Phys. Lett. B* **2014**, *730*, 99.
37. Meyer, H.B. A Calculation of the bulk viscosity in SU(3) gluodynamics. *Phys. Rev. Lett.* **2008**, *100*, 162001.
38. Mykhaylova, V.; Bluhm, M.; Redlich, K.; Sasaki, C. Quark-flavor dependence of the shear viscosity in a quasiparticle model. *Phys. Rev. D* **2019**, *100*, 034002.
39. Attems, M.; Casalderrey-Solana, J.; Mateos, D.; Papadimitriou, I.; Santos-Oliván, D.; Sopena, C.F.; Triana, M.; Zilhão, Z. Thermodynamics, transport and relaxation in non-conformal theories. *J. High Energy Phys.* **2016**, *1610*, 155.
40. Konchakovski, V.P.; Bratkovskaya, E.L.; Cassing, W.; Toneev, V.D.; Voronyuk, V. Rise of azimuthal anisotropies as a signature of the Quark–Gluon–Plasma in relativistic heavy-ion collisions. *Phys. Rev. C* **2012**, *85*, 011902.
41. Adamczyk, L.; Adams, J.R.; Adkins, J.K.; Agakishiev, G.; Aggarwal, M.M.; Ahammed, Z.; Ajitanand, N.N.; Alekseev, I.; Anderson, D.M.; Aoyama, R.; et al. Beam-Energy Dependence of Directed Flow of Λ , $\bar{\Lambda}$, K^\pm , K_s^0 and ϕ in Au+Au Collisions. *Phys. Rev. Lett.* **2018**, *120*, 062301.
42. Adams, J.; Aggarwal, M.M.; Ahammed, Z.; Amonett, J.; Anderson, B.D.; Arkhipkin, D.; Averichev, G.S.; Badyal, S.K.; Bai, Y.; Balewski, J.; et al. Azimuthal anisotropy in Au+Au collisions at $\sqrt{s_{NN}} = 200$ GeV. *Phys. Rev. C* **2005**, *72*, 014904.
43. Adamczyk, L.; Adkins, J.K.; Agakishiev, G.; Aggarwal, M.M.; Ahammed, Z.; Alekseev, I.; Aparin, A.; Arkhipkin, D.; Aschenauer, E.C.; Averichev, G.S.; et al. Centrality dependence of identified particle elliptic flow in relativistic heavy ion collisions at $\sqrt{s_{NN}} = 7.7\text{--}62.4$ GeV. *Phys. Rev. C* **2016**, *93*, 014907.
44. Back, B.B.; Baker, M.D.; Ballintijn, M.; Barton, D.S.; Betts, R.R.; Bickley, A.A.; Bindel, R.; Budzanowski, A.; Busza, W.; Carroll, A.; et al. Centrality and pseudorapidity dependence of elliptic flow for charged hadrons in Au+Au collisions at $\sqrt{s_{NN}} = 200$ GeV. *Phys. Rev. C* **2005**, *72*, 051901.

